ELECTRONIC PROPERTIES OF SOLID

Electron Spectrum and Heat Capacity of Heavy Fermions in the Canted Phase of Antiferromagnetic Intermetallides

V. V. Val'kov[a,b,c] and D. M. Dzebisashvili[a,b]

[a] *Institute of Physics, Siberian Branch, Russian Academy of Sciences, Krasnoyarsk, 660036 Russia*
[b] *Siberian Federal University, Krasnoyarsk, 660075 Russia*
[c] *Reshetnev Siberian State Aerospace University, Krasnoyarsk, 660014 Russia*
e-mail: vvv@iph.krasn.ru
Received June 4, 2009

Abstract—The energy spectrum of heavy fermions in an external magnetic field is calculated for canted magnetic sublattices of antiferromagnetic intermetallides. This makes it possible to determine low-temperature features of electronic heat capacity of heavy-fermion antiferromagnets with the metal-type ground state taking into account the structural rearrangement of the magnetic subsystem. The calculated temperature dependences of the magnetization, heat capacity, and Sommerfeld constant in the vicinity of the point of transition to the antiferromagnetic phase correlate with experimental data obtained for heavy-fermion antiferromagnets $PuGa_3$, Ce_2Au_2Cd, $YbNiSi_3$, and $PuPd_5Al_2$.

1. INTRODUCTION

The structure of the ground state (GS) and low-temperature properties of heavy fermion (HF) systems remain the objects of intense experimental and theoretical studies. The chemical composition of heavy-fermion compounds is based on rare-earth elements (mainly Ce and Yb) as well as U and transuranic elements (Pu and Np). It was found that the GS type in HF intermetallides may considerably change under the action of external fields.

The GS type is determined to a considerable extent by the result of competition of two interactions. On the one hand, the *s–f* exchange coupling between the spin moments of collectivized and localized *f* electrons exhibits a tendency toward screening of spin moments of localized electrons and to the formation of a nonmagnetic type of GS due to Kondo fluctuations. The exchange interaction between the spin moments of *f* electrons produces the opposite effect in its tendency to establish the magnetic order. A specific realization of the GS structure also depends on the relative position of the energy of a localized *f* level and the chemical potential.

If the *s–f* exchange interaction dominates in an intermetallide, it can be in a nonmagnetic metallic state characterized by a high value of Sommerfeld constant γ (a state with HFs). There are quite a large number of systems in which such a phase is observed at temperatures on the order of 10 K. However, it is only $CeCu_6$ (and probably $CePt_2Sn_2$) that remains a paramagnetic metal down to low temperatures [1]. In the remaining HF systems known at present, further modification of the ground state takes place at tempera-

tures on the order of 1 K. The formation of heavy quasiparticles may terminate, for example, by a transition from the metal to the semiconductor state, as in the case of CeNiSn [2], or to the dielectric state. A theory of low-temperature properties of such systems in weak magnetic fields was developed in [3]. Typical examples of HF dielectrics (so-called Kondo insulators) are the compounds $Ce_3Bi_4Pt_3$, SmB_6 [4], and $CeOs_4Sb_{12}$ [5]. The thermodynamic behavior of these systems is successfully described in the model of two-component Fermi liquid [6, 7].

Some intermetallic compounds with HF become superconducting at temperatures not exceeding 5 K. By way of example, we can consider classical HF superconductors such as $CeCu_2Si_2$ [8], UBe_{13} [9], UPt_3 [10], as well as recently discovered 1−1−5 $CeTIn_5$ systems (T stands for Co, Rh, or Ir) [11, 12] as well as skutterudites $LaFe_4P_{12}$ [13] and $PrRu_4As_{12}$ [14]. Sometimes, a transition to the superconducting phase occurs at a high pressure. For example, superconductivity in $CeRhIn_5$ [12] and $CeCu_2Ge_2$ [15] is observed only at pressures exceeding 16 and 77 kbar, respectively.

Finally, in a large number of HF systems, the exchange interaction between localized *f* electrons becomes predominant upon cooling. Such substances exhibit a phase transition with the formation of long-range magnetic order at temperatures on the order of 10 K. Ferromagnetic ordering takes place in UGe_2 [16], UIr [17], and $ZrZn_2$ [18] compounds. However, most magnetic HF systems are antiferromagnetic (AFM). In some HF compounds (like $CeRhIn_5$) [19], a change in external conditions induces a transition to

a state in which the AFM and superconducting (SC) order parameters coexist.

The variety of low-temperature phases and their modification by external effects initiates a large number of experimental studies of magnetic susceptibility [20], conductivity [21], magnetoresistance [22], thermopower [23], and heat capacity of HF systems under pressure and in an external magnetic field. In an analysis of the AFM phase of HF compounds in the vicinity of the phase transition, important information can be obtained from the processing of experimental data on the temperature evolution of heat capacity of $PuGa_3$ [24], Ce_2Au_2Cd [25], $YbNiSi_3$ [26], and $PuPd_5Al_2$ [27] in an external magnetic field. To correctly interpret the results of such experiments, the magnetic structure rearrangement induced by an external magnetic field must be adequately taken into account. This becomes obvious if we take into account the fact that the Néel temperature in HF antiferromagnets is relatively low ($T_N \sim 3$ K) [28], and a field of $H \sim 10^4$ Oe, which is commensurate to the parameter of exchange interaction between spin moments of f ions, causes considerable canting of magnetic sublattices.

However, the theoretical description of thermodynamic properties of AFM HF systems available in the literature is insufficient in many respects. For example, in [29−32], the Fermi spectrum of Kondo insulators in the strictly collinear AFM phase (in zero external magnetic field) was calculated using the symmetric periodic Anderson model (PAM). The energy spectrum of HF AFM metals in the canted face that form as the result of application of an external field has not been described as yet. At the same time, canting of magnetic sublattices and its variation with temperature lead to additional contributions to the electron heat capacity and change the Sommerfeld constant. This consequence alone stimulates the calculation of the low-temperature heat capacity of HF antiferromagnets with allowance for temperature-dependent canting of magnetic sublattices.

Theoretical analysis of the effects associated with long-range AFM order can be carried out using the extended PAM (EPAM) including exchange interactions in the subsystem of localized f electrons. This type of terms appears in the effective low-energy EPAM Hamiltonian in the regime of a strong but finite on-site Coulomb interaction U as a result of application of the unitary transformation method [33−36]. It should be noted, however, that the Schieffer–Wolf transformation [33, 34] cannot be directly applied to HF with metal-type conduction since the effective exchange integrals diverge when the localized level is in the conduction band [37]. Effective exchange interactions between the spin moments of f ions were derived in [38] using the Anderson model for the metal-type ground state; hybridization processes V_{12} associated with the participation of high-energy states of the upper Hubbard subband were singled out using

the atomic representation. This made it possible to construct the effective Hamiltonian of the EPAM up to the fourth order inclusively in parameter V_{12}/U and to derive explicit expressions for exchange integrals without any divergence.

In this study, the spectrum of heavy fermions in the AFM phase canted by an external magnetic field is calculated based using the effective Hamiltonian of the PAM in the regime of strong electron correlations. The solution to the problem is obtained on the basis of the slave-boson representation, which is widely used in the theory of heavy fermions and by successive application of five Bogolioubov transformations in the diagonalization of the quadratic form of the EPAM effective Hamiltonian. This enabled us to analyze the effect of the magnetic field on the temperature dependence of the heat capacity and the Sommerfeld constant of HF antiferromagnets.

2. EFFECTIVE HAMILTONIAN OF AFM INTERMETALLIDES

The EPAM Hamiltonian in the representation of creation $c_{k\sigma}^+$ ($d_{l\sigma}^+$) and annihilation $c_{k\sigma}$ ($d_{l\sigma}$) operators of a collectivized (localized) electron with quasi-momentum k (with Wannier cell number l) and spin moment projection σ has the form

$$
\begin{aligned}
\hat{\mathcal{H}} &= \sum_{k\sigma}(\varepsilon_{k\sigma} - \mu)c_{k\sigma}^+ c_{k\sigma} + \sum_{l\sigma}(E_\sigma - \mu)d_{l\sigma}^+ d_{l\sigma} \\
&+ U\sum_l \hat{n}_{l\uparrow}\hat{n}_{l\downarrow} + \frac{1}{\sqrt{N}}\sum_{lk\sigma}\{V_k e^{-ikl}c_{k\sigma}^+ d_{l\sigma} + \text{H.c.}\}.
\end{aligned}
\tag{1}
$$

The first sum describes noninteracting collectivized electrons in external magnetic field H removing the degeneracy of bare energy spectrum ε_k in spin moment—projections $\sigma = +1/2, -1/2$:

$$\varepsilon_{k\sigma} = \varepsilon_k - 2\sigma\mu_B H,$$

where μ_B is the Bohr magneton. The second term takes into account the presence of localized states with energy $E_\sigma = E_0 - g\sigma\mu_B H$, where E_0 is the bare energy. In the magnetic field, the localized energy level splits into two Zeeman sublevels. The splitting depends on the value of the g factor of the rare-earth ion. As usual, the introduction of chemical potential μ is associated with subsequent averaging over a large canonical ensemble. The Coulomb interaction of two electrons in the same ion is taken into account by the third term, in which $\hat{n}_{l\sigma} = d_{l\sigma}^+ d_{l\sigma}$ is the operator of the number of localized electrons with spin moment projection σ and U is the Hubbard repulsion energy. The last term in Eq. (1) describes hybridization processes of intensity V_k between two groups of electrons.

While determining the energy spectrum of heavy fermions in the canted AFM phase, we assume that localized level E_0 is in the lower half of the conduction

band. In the regime of strong electron correlations, energy $E_0 + U$ of the upper Hubbard level is above the top of the conduction band. If $U \gg |V_k|$, the use of the atomic representation for localized states of f ions makes it possible to explicitly separate high-energy hybridization processes with the participation of binary localized states from low-energy processes in the case when transitions of electrons from the conduction band occur only to localized states with one electron. Since the first hybridization processes occur with a level with a high value of $E_0 + U$, they can be taken into account using the operator form of perturbation theory. The implementation of such a program leads to the effective Hamiltonian including the exchange coupling of the spin moments of collectivized and localized electrons as well as the exchange interaction between the spin moments of f ions [38]. Thus, the physical properties of HF AFM intermetallides can be described using the modified Anderson Hamiltonian

$$\hat{\mathscr{H}} = \hat{\mathscr{H}}_0 + \hat{\mathscr{H}}_{\text{mix}} + \hat{\mathscr{H}}_{\text{exch}}, \qquad (2)$$

in which the terms are written in the two-sublattice Wannier representation. The first term in Eq. (2) takes into account the collectivized and localized states of electrons:

$$\hat{\mathscr{H}}_0 = \sum_{f\sigma}(\varepsilon_\sigma - \mu)a_{f\sigma}^+ a_{f\sigma} + \sum_{g\sigma}(\varepsilon_\sigma - \mu)b_{g\sigma}^+ b_{g\sigma}$$

$$+ \sum_{f\sigma}(E_\sigma - \mu)X_f^{\sigma\sigma} + \sum_{g\sigma}(E_\sigma - \mu)X_g^{\sigma\sigma}$$

$$+ \sum_{ff'\sigma}t_{ff'}a_{f\sigma}^+ a_{f'\sigma} + \sum_{gg'\sigma}t_{gg'}b_{g\sigma}^+ b_{g'\sigma} \qquad (3)$$

$$+ \sum_{fg\sigma}t_{fg}(b_{g\sigma}^+ a_{f\sigma} + a_{f\sigma}^+ b_{g\sigma}).$$

Subscripts f and f' denote the sites belonging to the F sublattice, while subscripts g and g' mark the sites corresponding to the G sublattice. The creation (annihilation) operators for conduction electrons belonging to the F and G sublattices will be redenoted as a_f^+ (a_f) and b_g^+ (b_g), respectively. The third and fourth terms in Eq. (3) describe the contributions of localized states from sublattices F and G, respectively. The fifth (sixth) sums in Eq. (3) describe the hoppings of conduction electrons in sublattice $F(G)$, while the last sum accounts for such hoppings between the sublattices. Quantity $\varepsilon_\sigma = \varepsilon - 2\sigma\mu_B H$ defines the diagonal part of the energy of the collectivized state in the Wannier representation in a magnetic field, ε in the bare level of the above energy, and $t_{ll'}$ are the matrix elements reflecting the intensity of hoppings of collectivized electrons from site l to site l' (site indices l and l' may correspond to the F as well as G sublattices). The states

of f ions are described in the atomic representation using the Hubbard operators

$$X_l^{m,\,n} = |m\rangle\langle n|.$$

For $n = 0$, vector $|n\rangle$ describes the state without electrons, while for $n = \sigma$ ($\sigma = \uparrow, \downarrow$) this vector describes the one-electron state with spin moment projection σ.

States with two f electrons at the same site do not participate in the formation of the Hilbert space of effective Hamiltonian (2) since processes involving binary states are taken into account using perturbation theory. This explains the fact that $\hat{\mathscr{H}}_{\text{mix}}$ contains only low-energy hybridization processes between localized and collectivized states:

$$\hat{\mathscr{H}}_{\text{mix}} = \sum_{fg\sigma}(W_{fg}a_{f\sigma}^+ X_g^{0\sigma} + W_{gf}b_{g\sigma}^+ X_f^{0\sigma})$$

$$+ \sum_{ff'\sigma}V_{ff'}a_{f\sigma}^+ X_{f'}^{0\sigma} + \sum_{gg'\sigma}V_{gg'}b_{g\sigma}^+ X_{g'}^{0\sigma} + \text{H.c.} \qquad (4)$$

The first sum in this relation describes hybridization processes between states from different sublattices with matrix elements W_{fg}. Hybridization processes within a sublattice are described by the second and third terms.

The exchange part of Hamiltonian (2), which is associated with virtual transition to binary states, can be written in the form

$$\hat{\mathscr{H}}_{\text{exch}} = \sum_{ff}J_{ff'}(\mathbf{S}_f \cdot \boldsymbol{\sigma}_f) + \sum_{gg'}J_{gg'}(\mathbf{S}_g \cdot \boldsymbol{\sigma}_{g'})$$

$$+ \sum_{fg}L_{fg}(\mathbf{S}_f \cdot \boldsymbol{\sigma}_g + \mathbf{S}_g \cdot \boldsymbol{\sigma}_f)$$

$$- \frac{1}{2}\sum_{ff'}I_{ff'}(\mathbf{S}_f \cdot \mathbf{S}_{f'}) - \frac{1}{2}\sum_{gg'}I_{gg'}(\mathbf{S}_g \cdot \mathbf{S}_{g'}) \qquad (5)$$

$$+ \sum_{fg}K_{fg}(\mathbf{S}_f \cdot \mathbf{S}_g).$$

Here, we have taken into account the s–f exchange interaction between the spin moments of localized and collectivized electrons, as well as the exchange interaction in the localized subsystem. The matrix elements for the s–f exchange interaction in the limits of the same sublattice are denoted by $J_{ff'}$ and $J_{gg'}$, while those for the same interaction from different sublattices are denoted by L_{fg}. Matrix elements $I_{ff'}$ and $I_{gg'}$ reflect the intensity of the exchange coupling between the spin moments of the localized states belonging to the same sublattice. The exchange integrals between the spin moments of localized stated from different sublattices are denoted by K_{fg}. The behavior of the exchange parameters upon a change in hybridization
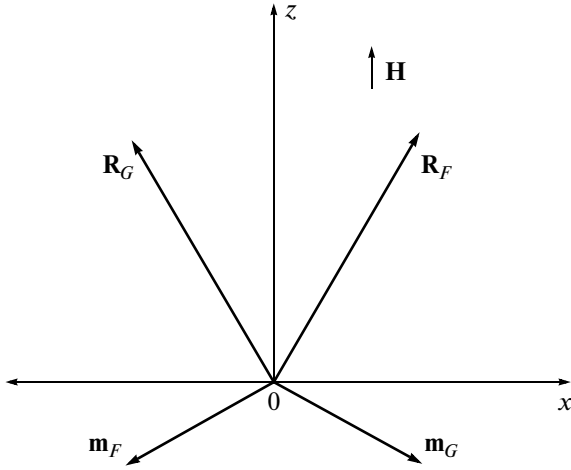
Fig. 1. Direction of magnetization vectors in the canted phase upon the application of magnetic field **H** along the z axis. For $\mathbf{H} = 0$, all vectors are collinear to the x axis.

and the distance between lattice sites are analyzed in [38].

The components of localized quasi-spin operators $\mathbf{S}_l$ are connected with the Hubbard operators via familiar relations

$$S_l^x = \frac{1}{2}\sum_\sigma X_l^{\sigma\bar\sigma}, \quad S_l^y = i\sum_\sigma \sigma X_l^{\bar\sigma\sigma},$$

$$S_l^z = \sum_\sigma \sigma X_l^{\sigma\sigma}, \quad S_l^+ = X_l^{\uparrow\downarrow}, \tag{6}$$

$$S_l^- = X_l^{\downarrow\uparrow} \quad (\bar\sigma = -\sigma).$$

For collectivized states, the relations between the components of the electron spin operator and the Fermi operator have the form

$$\sigma_l^x = (c_{l\uparrow}^+ c_{l\downarrow} + c_{l\downarrow}^+ c_{l\uparrow})/2, \quad \sigma_l^y = (c_{l\uparrow}^+ c_{l\downarrow} - c_{l\downarrow}^+ c_{l\uparrow})/2i,$$

$$\sigma_l^z = (c_{l\uparrow}^+ c_{l\uparrow} - c_{l\downarrow}^+ c_{l\downarrow})/2.$$

3. SLAVE-BOSON REPRESENTATION AND DIAGONALIZATION OF HAMILTONIAN IN THE MEAN-FIELD APPROXIMATION FOR CANTED AFM PHASE IN A MAGNETIC FIELD

In a magnetic field, the magnetic structure of an HF antiferromagnet is deformed, and equilibrium magnetization vectors $\mathbf{R}_F$ and $\mathbf{R}_G$ in the F and G sublattices are oriented relative to each other at an angle differing from 180° (Fig. 1). This canting of the magnetic sublattices due to the s–f exchange coupling of localized and collectivized spins induces a rearrangement of the Fermi excitation spectrum. As a result, the dependence of the electron heat capacity on the external magnetic field contains renormalizations associ-

ated with the magnetic field dependence of the cant of the magnetic sublattices.

We will analyze the above effects in the approximation disregarding relaxation processes. In this case, the effect of the localized subsystem on the collectivized one can be described in the mean-field approximation. Hybridization processes will be taken into account in the slave-boson representation using the average constraint at a latter stage [39]. It is well known that such an approach provides a satisfactory description for the energy spectrum of heavy fermions in the nonmagnetic phase. This allows us to represent the EPAM Hamiltonian in the form

$$\hat{\mathcal{H}} = \hat{\mathcal{H}}_c + \hat{\mathcal{H}}_L + \hat{\mathcal{H}}_{\mathrm{mix}} + C, \tag{7}$$

where $\hat{\mathcal{H}}_c$ is the Hamiltonian of the collectivized subsystem,

$$\hat{\mathcal{H}}_c = \sum_{k\sigma} \{[t_k + \sigma(J_0 + L_0)R_\parallel - 2\sigma\mu_B H]$$

$$\times (a_{k\sigma}^+ a_{k\sigma} + b_{k\sigma}^+ b_{k\sigma}) + \Gamma_k(a_{k\sigma}^+ b_{k\sigma} + b_{k\sigma}^+ a_{k\sigma}) \tag{8}$$

$$+ [(J_0 - L_0)R_\perp/2](a_{k\sigma}^+ a_{k\bar\sigma} - b_{k\sigma}^+ b_{k\bar\sigma})\},$$

and the Fourier transforms of hopping integrals are defined for the Brillouin zone corresponding to the AFM phase:

$$t_{ff'} = N^{-1}\sum_k t_k \exp\{ik(f-f')\},$$

$$t_{fg} = N^{-1}\sum_k \Gamma_k \exp\{ik(f-g)\},$$

where N is the number of sites in the magnetic sublattice. The effect of the localized subsystem is manifested in the form of magnetizing field $\sim R_\parallel = \langle S_f^z \rangle = \langle S_g^z \rangle$ as well as the term $\sim R_\perp = \langle S_f^x \rangle = -\langle S_g^x \rangle$ describing processes with the flip of the spin moment projection in the collectivized subsystem.

After the two-stage Bogoliubov transformation

$$a_{k\sigma} = (\alpha_{k\sigma} - \beta_{k\sigma})/\sqrt{2},$$

$$b_{k\sigma} = (\alpha_{k\sigma} + \beta_{k\sigma})/\sqrt{2},$$

$$\alpha_{k\sigma} = \cos\varphi_{k\sigma}A_{k\sigma} - \sin\varphi_{k\sigma}B_{k\bar\sigma}, \tag{9}$$

$$\beta_{k\bar\sigma} = \cos\varphi_{k\sigma}B_{k\bar\sigma} + \sin\varphi_{k\sigma}A_{k\sigma}$$

with transformation parameters

$$\cos 2\varphi_{k\sigma} = -\Gamma_{k\sigma}/\nu_{k\sigma}, \quad \sin 2\varphi_{k\sigma} = \Delta_\perp/\nu_{k\sigma},$$

$$\Delta_\perp = (J_0 - L_0)/R_\perp/2,$$

$$\Gamma_{k\sigma} = \Gamma_k + \sigma[(J_0 + L_0)R_\parallel - 2\mu_B H], \tag{10}$$

$$\nu_{k\sigma} = \sqrt{\Gamma_{k\sigma}^2 + \Delta_\perp^2}$$

operator (8) assumes the diagonal form

$$\hat{\mathcal{H}}_c = \sum_{k\sigma} \{\xi_{k\sigma}^- A_{k\sigma}^+ A_{k\sigma} + \xi_{k\bar{\sigma}}^+ B_{k\bar{\sigma}}^+ B_{k\bar{\sigma}}\}, \tag{11}$$

$$\xi_{k\sigma}^\pm = t_k \pm \nu_{k\sigma}.$$

Using the slave-boson representation [39] for the Hubbard operators of the localized subsystem, we denote the Fermi operators for the F sublattice by $\Lambda_{f\sigma}$, whereas the Fermi operators for the G sublattice will be denoted by $\chi_{g\sigma}$. Taking into account the mean-field effects induced by the action of exchange interactions on the localized states, we obtain the Hamiltonian of the localized subsystem in the quasi-momentum representation:

$$\hat{\mathcal{H}}_L = \sum_{k\sigma} \left\{ (E_0 + \lambda + \sigma h_\|)(\Lambda_{k\sigma}^+ \Lambda_{k\sigma} + \chi_{k\sigma}^+ \chi_{k\sigma}) \right.$$
$$\left. - \frac{h_\perp}{2}(\Lambda_{k\sigma}^+ \Lambda_{k\bar{\sigma}} - \chi_{k\sigma}^+ \chi_{k\bar{\sigma}}) \right\}. \tag{12}$$

Here, $h_\| = -g\mu_B H + m_\|(J_0 + L_0) + R_\|(K_0 - I_0)$, $h_\perp = R_\perp(K_0 + I_0) - m_\perp(J_0 - L_0)$, $m_\| = \langle \sigma_f^z \rangle = \langle \sigma_g^z \rangle$, and $m_\perp = \langle \sigma_f^x \rangle = -\langle \sigma_g^x \rangle$. Parameter λ defines the renormalization of energy of the localized level emerging when the slave-boson representation is used [39].

The diagonalization of $\hat{\mathcal{H}}_L$ is carried out via the transformation

$$\Lambda_{k\sigma} = \cos\phi D_{k\sigma} + 2\sigma \sin\phi D_{k\bar{\sigma}},$$
$$\chi_{k\sigma} = \cos\phi G_{k\sigma} - 2\sigma \sin\phi G_{k\bar{\sigma}}, \tag{13}$$

where angle ϕ satisfies the following conditions:

$$\cos 2\phi = -\frac{h_\|}{\overline{H}_\Lambda}, \quad \sin 2\phi = -\frac{h_\perp}{\overline{H}_\Lambda}, \tag{14}$$

$$\overline{H}_\Lambda = \sqrt{h_\perp^2 + h_\|^2}.$$

This gives the following expression for $\hat{\mathcal{H}}_L$:

$$\hat{\mathcal{H}}_L = \sum_{k\sigma} \tilde{E}_\sigma (D_{k\sigma}^+ D_{k\sigma} + G_{k\sigma}^+ G_{k\sigma}), \tag{15}$$

where $\tilde{E}_\sigma = E_0 + \lambda - \sigma \overline{H}_\Lambda$ is the energy of localized electrons in the canted phase disregarding hybridization processes.

In the approach used here, the term $\hat{\mathcal{H}}_{\mathrm{mix}}$ has the form

$$\hat{\mathcal{H}}_{\mathrm{mix}} = \sum_{k\sigma} \{\tilde{V}_k(a_{k\sigma}^+ \Lambda_{k\sigma} + b_{k\sigma}^+ \chi_{k\sigma})$$
$$+ \tilde{W}_k(a_{k\sigma}^+ \chi_{k\sigma} + b_{k\sigma}^+ \Lambda_{k\sigma})\} + \text{H.c.}, \tag{16}$$

where $\tilde{V}_k = e_0 V_k$, $\tilde{W}_k = e_0 W_k$, and e_0^2 is the mean value of the operator of the number of auxiliary bosons per site. The Fourier transforms of the intra- and intersublattice hybridization parameters are also defined for the magnetic Brillouin zone:

$$V_k = \sum_{(f-f')} V_{ff'} \exp\{-ik(f-f')\},$$

$$W_k = \sum_{(f-g)} W_{fg} \exp\{-ik(f-g)\}.$$

As a result of application of transformations (9) and (13), the equations of motion taking into account operator $\hat{\mathcal{H}}_{\mathrm{mix}}$ form a closed eighth-degree nondecomposable system. Accordingly, the dispersion equation is also an eighth-degree equation, and the derivation of closed self-consistent equations becomes cumbersome.

The situation is radically simplified if we introduce one more unitary transformation:

$$D_{k\sigma} = \frac{1}{\sqrt{2}}(P_{k\sigma} + L_{k\sigma}),$$
$$G_{k\sigma} = \frac{1}{\sqrt{2}}(P_{k\sigma} - L_{k\sigma}). \tag{17}$$

In this case, the hybridization part of Hamiltonian (2) assumes the form

$$\hat{\mathcal{H}}_{\mathrm{mix}} = \sum_{k\sigma} \{(v_{+,k\sigma}^{(c)} A_{k\sigma}^+ - v_{+,k\sigma}^{(s)} B_{k\bar{\sigma}}^+) P_{k\sigma}$$
$$- (v_{-,k\sigma}^{(s)} A_{k\sigma}^+ + v_{-,k\sigma}^{(c)} B_{k\bar{\sigma}}) L_{k\bar{\sigma}}\} + \text{H.c.}, \tag{18}$$

where $v_{\pm,k\sigma}^{(c)} = \tilde{V}_k \cos\psi_{k\sigma}^- \pm \tilde{W}_k \cos\psi_{k\sigma}^+$, $v_{\pm,k\sigma}^{(s)} = \tilde{V}_k \sin\psi_{k\sigma}^- \pm \tilde{W}_k \sin\psi_{k\sigma}^+$, $\psi_{k\sigma}^\pm = \varphi_{k\sigma} \pm 2\sigma\phi$. However, the structure of $\hat{\mathcal{H}}_L$ does not change as a result of transformation (17):

$$\hat{\mathcal{H}}_L = \sum_{k\sigma} \tilde{E}_\sigma (P_{k\sigma}^+ P_{k\sigma} + L_{k\sigma}^+ L_{k\sigma}). \tag{19}$$

It is significant that the equations of motion are now decomposed into two independent fourth-degree blocks.

Constant C in Hamiltonian (7) contains mean-field corrections to the energy of the system, as well as the term associated with constraint imposed on the number of localized electrons ($n_f \le 1$):

$$C = -2NR_\| m_\|(J_0 + L_0) - 4Nm_\perp \Delta_\perp$$
$$+ NR_\perp^2(K_0 + I_0) + NR_\|^2(I_0 - K_0) + 2N\lambda(e_0^2 - 1). \tag{20}$$

For final diagonalization of the quadratic form of the EPAM Hamiltonian, which is defined by expres-

sions (11), (18), and (19), we apply the fifth unitary transformation ($\lambda = 1, ..., 4$)

$$Z_{\lambda k\sigma} = u_{\lambda 1, k\sigma} A_{k\sigma} + u_{\lambda 2, k\sigma} B_{k\bar{\sigma}}$$
$$+ u_{\lambda 3, k\sigma} P_{k\sigma} + u_{\lambda 4, k\sigma} L_{k\bar{\sigma}}. \tag{21}$$

Coefficients $u_{\lambda j, k\sigma}$ of this transformation can be determined from the requirement of the diagonal form of the operator part of the EPAM Hamiltonian in the representation of new operators $Z_{\lambda k\sigma}$:

$$\hat{\mathcal{H}}_c + \hat{\mathcal{H}}_{\mathrm{mix}} + \hat{\mathcal{H}}_L = \sum_{\lambda k\sigma} E_{\lambda k\sigma} Z^+_{\lambda k\sigma} Z_{\lambda k\sigma}. \tag{22}$$

This requirement boils down to the solution of the system of four homogeneous equations:

$$\begin{pmatrix} \omega - \xi^-_{k\sigma} & 0 & -(v^{(c)}_{+,k\sigma})^* & (v^{(s)}_{-,k\sigma})^* \\ 0 & \omega - \xi^+_{k\sigma} & (v^{(s)}_{+,k\sigma})^* & (v^{(c)}_{-,k\sigma})^* \\ -v^{(c)}_{+,k\sigma} & v^{(s)}_{+,k\sigma} & \omega - E_\sigma & 0 \\ v^{(s)}_{-,k\sigma} & v^{(c)}_{-,k\sigma} & 0 & \omega - E_{k\bar{\sigma}} \end{pmatrix}$$

$$\times \begin{pmatrix} u_{\lambda 1, k\sigma} \\ u_{\lambda 2, k\sigma} \\ u_{\lambda 3, k\sigma} \\ u_{\lambda 4, k\sigma} \end{pmatrix} = 0. \tag{23}$$

Using the condition for the existence of nontrivial solutions of the given system, we obtain the dispersion equation defining eight branches $E_{\lambda k\sigma}$ ($\lambda = 1, ..., 4$, $\sigma = \pm 1/2$) of the Fermi excitation spectrum of EPAM in the canted AFM phase:

$$(\omega - \xi^-_{k\sigma})(\omega - \xi^+_{k\sigma})(\omega - E_\sigma)(\omega - E_{\bar{\sigma}})$$
$$+ \left| \tilde{V}^2_k - \tilde{W}^2_k \right|^2 - (\omega - \xi^-_{k\sigma})(\omega - E_{\bar{\sigma}}) \left| v^{(s)}_{+,k\sigma} \right|^2$$
$$- (\omega - \xi^-_{k\sigma})(\omega - E_\sigma) \left| v^{(c)}_{-,k\sigma} \right|^2 - (\omega - \xi^+_{k\sigma})(\omega - E_\sigma) \tag{24}$$
$$\times \left| v^{(s)}_{-,k\sigma} \right|^2 - (\omega - \xi^+_{k\sigma})(\omega - E_{\bar{\sigma}}) \left| v^{(c)}_{+,k\sigma} \right|^2 = 0.$$

In the particular case with allowance for only the intrasublattice hybridization ($V_k \neq 0$, $W_k = 0$), the dispersion equation is simplified as follows:

$$[(\omega - \xi^-_{k\sigma})(\omega - E_\sigma) - |\tilde{V}_k|^2]$$
$$\times [(\omega - \xi^+_{k\sigma})(\omega - E_{\bar{\sigma}}) - |\tilde{V}_k|^2] \tag{25}$$
$$+ 4\sigma |\tilde{V}_k|^2 \sin^2 \psi^-_{k\sigma} \bar{H}_\Lambda \nu_{k\sigma} = 0.$$

In the opposite situation ($W_k \neq 0$, $V_k = 0$), the dispersion equation has the form

$$[(\omega - \xi^-_{k\sigma})(\omega - E_\sigma) - |\tilde{W}_k|^2]$$
$$\times [(\omega - \xi^+_{k\sigma})(\omega - E_{\bar{\sigma}}) - |\tilde{W}_k|^2] \tag{26}$$
$$+ 4\sigma |\tilde{W}_k|^2 \sin^2 \psi^+_{k\sigma} \bar{H}_\Lambda \nu_{k\sigma} = 0.$$

Equations (25) and (26) formally differ only in the argument of the sine in the last term. In the paraphrase ($\bar{H}_\Lambda = 0$), both these equations give the standard mixion spectrum.

To simplify analytic calculations, we will confine further analysis to the case of one-sublattice hybridization ($W_k = 0$). For determining the coefficients of transformation (21), we will use, in addition to Eqs. (23), the unitarity condition $\sum_j u^2_{\lambda j, k_\sigma} = 1$. This gives the following expression for the coefficients of the fifth transformation:

$$u_{\lambda 1, k\sigma} = \{-(E_{\lambda k\sigma} - \xi^+_{k\sigma})(E_{\lambda k\sigma} - E_\sigma)$$
$$\times (E_{\lambda k\sigma} - E_{\bar{\sigma}}) + |\tilde{V}_k|^2 \cos^2 \psi^-_{k\sigma}(E_{\lambda k\sigma} - E_\sigma)$$
$$+ |\tilde{V}_k|^2 \sin^2 \psi^-_{k\sigma}(E_{\lambda k\sigma} - E_{\bar{\sigma}}) \} / \Delta_{k\sigma}(E_{\lambda k\sigma}),$$

$$u_{\lambda 2, k\sigma} = |\tilde{V}_k|^2 \sin \psi^-_{k\sigma}$$
$$\times \cos \psi^-_{k\sigma}(E_{\bar{\sigma}} - E_\sigma) / \Delta_{k\sigma}(E_{\lambda k\sigma}), \tag{27}$$

$$u_{\lambda 3, k\sigma} = |\tilde{V}_k| \cos \psi^-_{k\sigma} \{|\tilde{V}_k|^2 - (E_{\lambda k\sigma} - \xi^+_{k\sigma})$$
$$\times (E_{\lambda k\sigma} - E_{\bar{\sigma}}) \} / \Delta_{k\sigma}(E_{\lambda ks\sigma}),$$

$$u_{\lambda 4, k\sigma} = |\tilde{V}_k| \sin \psi^-_{k\sigma} \{|\tilde{V}_k|^2 - (E_{\lambda k\sigma} - \xi^+_{k\sigma})$$
$$\times (E_{\lambda k\sigma} - E_\sigma) \} / \Delta_{k\sigma}(E_{\lambda k\sigma}),$$

where

$$\Delta^2_{k\sigma}(\omega) = \cos^2 \psi^-_{k\sigma} \left[(\omega - E_\sigma)^2 + |\tilde{V}_k|^2 \right]$$
$$\times \left[|\tilde{V}_k|^2 - (\omega - E_{\bar{\sigma}})(\omega - \xi^+_{k\sigma}) \right]^2$$
$$+ \sin^2 \psi^-_\sigma \left[(\omega - E_{\bar{\sigma}})^2 + |\tilde{V}_k|^2 \right]$$
$$\times \left[|\tilde{V}_k|^2 - (\omega - E_\sigma)(\omega - \xi^+_{k\sigma}) \right]^2.$$

Introducing the function

$$\Phi^{ij}_{\lambda k\sigma}(\alpha) = (u^*_{\lambda i, k\sigma} \cos \alpha + u^*_{\lambda j, k\sigma} \sin \alpha)/\sqrt{2},$$
$$i, j = 1, 2, 3, 4,$$

we express the initial operators of the EPAM effective Hamiltonian in terms of operators $Z_{\lambda k\sigma}$; in the representation of these operators, the Hamiltonian has the diagonal form (see Eq. (22))

$$a_{k\sigma} = \sum_\lambda [\Phi^{12}_{\lambda k\sigma}(-\varphi_{k\sigma}) Z_{\lambda k\sigma} - \Phi^{21}_{\lambda k\bar{\sigma}}(\varphi_{k\bar{\sigma}}) Z_{\lambda k\bar{\sigma}}],$$

$$b_{k\sigma} = \sum_\lambda [\Phi^{12}_{\lambda k\sigma}(-\varphi_{k\sigma}) Z_{\lambda k\sigma} + \Phi^{21}_{\lambda k\bar{\sigma}}(\varphi_{k\bar{\sigma}}) Z_{\lambda k\bar{\sigma}}],$$

$$\tag{28}$$

$$\Lambda_{k\sigma} = \sum_\lambda [\Phi^{34}_{\lambda k\sigma}(2\sigma\phi) Z_{\lambda k\sigma} + \Phi^{43}_{\lambda k\bar{\sigma}}(2\sigma\phi) Z_{\lambda k\bar{\sigma}}],$$

$$\chi_{k\sigma} = \sum_{\lambda}[\Phi_{\lambda k\sigma}^{34}(2\sigma\phi)Z_{\lambda k\sigma} - \Phi_{\lambda k\bar{\sigma}}^{43}(2\sigma\phi)Z_{\lambda k\bar{\sigma}}].$$

4. SELF-CONSISTENT EQUATIONS

Diagonalization of the Hamiltonian with the help of transformation (28) makes it possible to calculate all of the mean values of the initial operators. This is necessary for deriving a system of integral equations for seven matching parameters: μ, λ, $R_{\parallel}$, $m_{\parallel}$, e_0, $R_{\perp}$, and $m_{\perp}$. For example, the expressions for the distribution functions of localized and collectivized electrons have the form

$$\langle \Lambda_{k\sigma}^{+}\Lambda_{k\sigma}\rangle = \sum_{\lambda}\left|\Phi_{\lambda k\sigma}^{34}(2\sigma\phi)\right|^2 f(E_{\lambda k\sigma})$$
$$+ \sum_{\lambda}\left|\Phi_{\lambda k\bar{\sigma}}^{43}(2\sigma\phi)\right|^2 f(E_{\lambda k\bar{\sigma}}), \tag{29}$$

$$\langle a_{k\sigma}^{+}a_{k\sigma}\rangle = \sum_{\lambda}\left|\Phi_{\lambda k\sigma}^{12}(-\phi_{k\sigma})\right|^2 f(E_{\lambda k\sigma})$$
$$+ \sum_{\lambda}\left|\Phi_{\lambda k\bar{\sigma}}^{21}(\phi_{k\bar{\sigma}})\right|^2 f(E_{\lambda k\bar{\sigma}}), \tag{30}$$

where $f(x) = 1/(\exp((x - \mu)/T) + 1)$ is the Fermi–Dirac distribution function. In view of the equivalence of magnetic sublattices, we have

$$\langle \Lambda_{k\sigma}^{+}\Lambda_{k\sigma}\rangle = \langle \chi_{k\sigma}^{+}\chi_{k\sigma}\rangle, \quad \langle a_{k\sigma}^{+}a_{k\sigma}\rangle = \langle b_{k\sigma}^{+}b_{k\sigma}\rangle.$$

Correlation functions (29) and (30) are used in the first four matching equations for parameters μ, λ, $R_{\parallel}$, and $m_{\parallel}$,

$$n = 2\frac{1}{N}\sum_{k\sigma}(\langle \Lambda_{k\sigma}^{+}\Lambda_{k\sigma}\rangle + \langle a_{k\sigma}^{+}a_{k\sigma}\rangle),$$

$$\frac{1}{N}\sum_{k\sigma}\langle \Lambda_{k\sigma}^{+}\Lambda_{k\sigma}\rangle = 1 - e_0^2,$$
$$\tag{31}$$
$$R_{\parallel} = \frac{1}{N}\sum_{k\sigma}\sigma\langle \Lambda_{k\sigma}^{+}\Lambda_{k\sigma}\rangle,$$

$$m_{\parallel} = \frac{1}{N}\sum_{k\sigma}\sigma\langle a_{k\sigma}^{+}a_{k\sigma}\rangle,$$

where n is the total number of electrons in the system.

It is well known that in the description of heavy fermions with the help of slave bosons, the effective value of hybridization becomes a function of external parameters (temperature, magnetic field, and so on) [39]. This dependence appears due to renorm factor e_0^2 appearing in the hybridization parameter in the equations for the Green functions and, as a consequence, in the matching equations. The equation for

this renorm factor can usually be derived from the condition of the free energy minimum. In our case, this equation has the form

$$-\lambda e_0 = \frac{1}{N}\sum_{\lambda k\sigma}V_k[(\Phi_{\lambda k\sigma}^{12}(-\phi_{k\sigma}))^*\Phi_{\lambda k\sigma}^{24}(2\sigma\phi)f(E_{\lambda k\sigma})$$
$$\tag{32}$$
$$-(\Phi_{\lambda k\bar{\sigma}}^{21}(\phi_{k\bar{\sigma}}))^*\Phi_{\lambda k\bar{\sigma}}^{43}(2\sigma\phi)f(E_{\lambda k\bar{\sigma}})].$$

The remaining two order parameters $R_{\perp}$ and $m_{\perp}$, which define the transverse magnetization components for localized and collectivized electrons, can be determined from the solution of the matching equations:

$$R_{\perp} = \frac{1}{2}\frac{1}{N}\sum_{k\sigma}\langle \Lambda_{k\sigma}^{+}\Lambda_{k\bar{\sigma}}\rangle,$$
$$\tag{33}$$
$$m_{\perp} = \frac{1}{2}\frac{1}{N}\sum_{k\sigma}\langle a_{k\sigma}^{+}a_{k\bar{\sigma}}\rangle,$$

where the mean values can be written, taking into account relation (28), in the form

$$\langle a_{k\sigma}^{+}a_{k\bar{\sigma}}\rangle = -\sum_{\lambda}(\Phi_{\lambda k\sigma}^{12}(-\phi_{k\sigma}))^*\Phi_{\lambda k\sigma}^{21}(\phi_{k\sigma})f(E_{\lambda k\sigma})$$
$$\tag{34}$$
$$-\sum_{\lambda}(\Phi_{\lambda k\bar{\sigma}}^{21}(\phi_{k\bar{\sigma}}))^*\Phi_{\lambda k\bar{\sigma}}^{12}(-\phi_{k\bar{\sigma}})f(E_{\lambda k\bar{\sigma}}),$$

$$\langle \Lambda_{k\sigma}^{+}\Lambda_{k\bar{\sigma}}\rangle = \sum_{\lambda}(\Phi_{\lambda k\sigma}^{34}(2\sigma\phi))^*\Phi_{\lambda k\sigma}^{43}(-2\sigma\phi)f(E_{\lambda k\sigma})$$
$$\tag{35}$$
$$+\sum_{\lambda}(\Phi_{\lambda k\bar{\sigma}}^{43}(2\sigma\phi))^*\Phi_{\lambda k\bar{\sigma}}^{34}(-2\sigma\phi)f(E_{\lambda k\bar{\sigma}}).$$

Equations (31)–(35) form the system of seven integral equations, which will be subsequently used for self-consistent calculation of the low-temperature thermodynamics of HF intermetallides with the AFM phase canted by the magnetic field.

5. STRUCTURE OF THE GROUND STATE AND THE EPAM FERMI EXCITATION SPECTRUM IN THE CANTED AFM PHASE

In numerical calculations, we assumed that ordering of ions corresponds to a body-centered cubic (bcc) lattice, while the bare conduction band is formed due to hoppings between nearest neighbors with tunnel integral t_1. In this case,

$$\Gamma_k = 8t_1\cos\left(\frac{k_x b}{2}\right)\cos\left(\frac{k_y b}{2}\right)\cos\left(\frac{k_z b}{2}\right),$$
$$\tag{36}$$
$$t_k = 0,$$

where b is the magnetic lattice parameter. To simplify calculations, we took into account only the s–f exchange processes between localized and collectivized electron states occurring within a cell. An analogous simplification was also made for hybridization
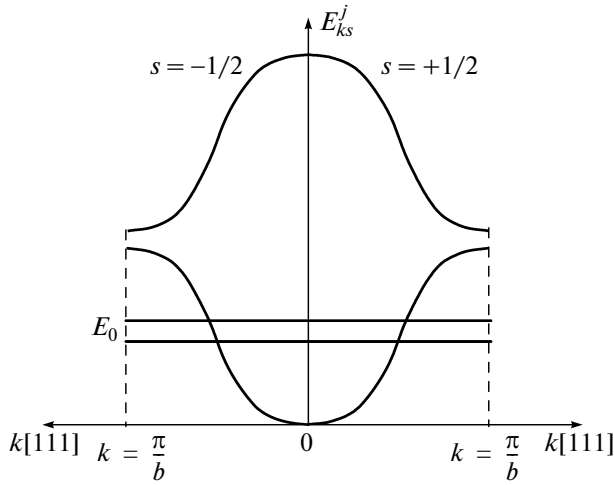
Fig. 2. Qualitative form of the bare band structure in the EPAM for the AFM phase.

processes. These constraints lead to the following equalities: $V_q = V$, $W_q = 0$, $J_q = J$, and $L_q = 0$, where V and J are the values of the hybridization parameter and $s-f$ exchange integral, respectively. To eliminate frustration effects in the localized electron subsystem, we assumed that the exchange coupling takes place only between the nearest spins from different sublattices. Thus, $I_q = 0$ and $K_q = 8K_1\cos(q_x b/2)\cos(q_y b/2)\cos(q_z b/2)$, where K_1 is the exchange integral for the nearest neighbors. All energy parameters will be henceforth measured in the units of $|t_1|$ ($t_1 < 0$).

As the starting point, we consider schematically the Fermi excitation spectrum in the AFM phase for $H = 0$. This spectrum is determined by the solutions to dispersion equation (25) and is shown qualitatively in Fig. 2 disregarding hybridization. The right and left sides of the figure show the spectrum for $\sigma = +1/2$ and $-1/2$, respectively. Four spectral branches $E_{\lambda k \sigma}$ ($\lambda = 1$, 2, 3, 4) are degenerate in quantum number σ (the left and right branches in the figure are identical). The straight lines correspond to the energy levels of localized states of the f subsystem with bare energy E_0, which are split by exchange field $\overline{H}_\Lambda$. For better visualization, the splitting of levels is enlarged in Fig. 2. In actual practice, the value of $\overline{H}_\Lambda$ is two or three orders of magnitude smaller than the bandwidth. The dispersion curves describe the bare spectrum of collectivized electrons. Doubling of the number of branches as compared to the paramagnetic case is due to the AFM structure for which the corresponding decrease in the Brillouin zone width takes place. In the case considered here, the quasi-momentum varies along the [111] direction. For other directions, the pattern is qualitatively the same.

In the further analysis, we will confine ourselves to the case when the localized level, as in Fig. 2, is within the lower half of the bare band of collectivized electrons and the chemical potential is in the immediate vicinity of this level. Since the effective field $\overline{H}_\Lambda$ determining the splitting energy of f states is much smaller than the conduction band width, the most significant changes occur in the energy spectrum under the action of hybridization processes and canting of magnetic sublattices only in the vicinity of energy E_0. For this reason, considering the effect of the magnetic field, we will accentuate attention only on the modification of the Fermi spectrum in the immediate vicinity of this energy region. Such analysis is of special importance since modification of energy spectrum in this region is responsible for all peculiarities of the low-temperature thermodynamics of heavy fermions in the AFM canted phase, while the uppermost spectral branches with $\lambda = 4$ make zero contribution to the thermodynamic parameters of the system.

Before we pass to analysis of dispersion relations calculated self-consistently, let us consider the features of the temperature dependence of the key parameter in the theory of slave bosons, viz., e_0^2. It has been reliably established that the self-consistent solution of equations for e_0^2 in the paramagnetic phase leads to a monotonic decrease in this parameter. The theory acquires an important energy parameter T^* defining the temperature at which e_0^2 vanishes. At $T < T^*$, the system is in a coherent regime. In the approximation of a rectangular density of Fermi states with band half-width D, we have

$$T^* = 2\frac{e^C}{\pi}\sqrt{D^2 - \mu^2}\exp\left\{-\frac{\lambda D}{V^2}\right\},$$

where $C = 0.577$ is the Euler constant. In this case, the Kondo temperature considerably exceeds T^*.

Self-consistent calculations show that the situation slightly changes in the presence of exchange interactions between localized spin moments and after the emergence of long-range magnetic order. This is because the system acquires a new energy scale (Néel temperature T_N in our case). It turns out that the temperature dependence of e_0^2 in the magnetically ordered phase increases monotonically. This situation is illustrated in Fig. 3, obtained as a result of self-consistent solution of the above system of integral equations for the following values of the parameters: $E_0 = -4$, $V = 0.53$, $K_0 = 0.002$, $J_0 = 0.002$, and $n = 2.4$. It can be seen that at the point of magnetic ordering, the temperature dependence of e_0^2 changes and passes to the typically paramagnetic behavior. The Néel temperature in this case is always lower than the coherence temperature. It should be emphasized that this dependence is typi-

cal and is observed for other values of model parameters as well.

Figure 4 shows the spectrum for the AFM phase in the vicinity of a localized level, which was calculated using dispersion equation (25) and system of self-consistent equations (31)−(35) for three temperature values. The model parameters were chosen as follows: $E_0 = -4$, $V = 0.4$, $K_0 = 0.02$, $J_0 = 0.5$, $n = 2.2$, and magnetic field $H = 0$. The value of the Néel temperature of 23 K given in the figure ($T_N = 14.5$ K for UPd$_2$Al$_3$ [40] and $T_N = 35$ K for CeRh$_2$Si$_2$ [41]) corresponds to a bare conduction band width of 16 eV ($|t_1| = 1$ eV). If we choose smaller values of the bandwidth, the Néel temperature will decrease in the same proportion. Analogous scaling of energy values will be used in the figures below. The most significant feature of this spectrum is the presence of a narrow band of heavy quasiparticles separated by gaps from the upper and lower bands. This pattern of the spectrum basically differs from the spectral structure of HFs in the paramagnetic phase, for which the energy spectrum of heavy quasiparticles is separated by an energy gap only from one side.

The width of the split band of HFs is on the order of $\overline{H}_\Lambda$; it can be seen from conditions (14) that it is defined by the values of magnetic parameters of the localized and collectivized subsystems. Figure 4b shows the corresponding density of electron states in the vicinity of the localized level on the same energy scale as for the spectrum in Fig. 4a.

Comparing Figs. 4c−4f with Figs. 4a and 4b, we can trace the temperature evolution of the band structure. In particular, it can be seen that with increasing temperature, the width of the narrow band gradually decreases, while the chemical potential, which was initially inside this band, decreases to a value below the bottom of this band. At a temperature on the order of 19 K, the narrow band degenerates into a level, and a further increase in temperature leads to inversion of this band (see Fig. 4c). As a result of inversion, the dispersion peak of the narrow band ($E_{2k\sigma}$) corresponds to a state at the center of the Brillouin zone. The inversion of the narrow band is accompanied by a considerable decrease in the average magnetization R of localized electrons. As the temperature approaches T_N, the lower gap (between the bands with $\lambda = 1$ and 2) decreases and disappears (see Figs. 4e and 4f), while the upper gap (hybridization gap of the paraphrase) is preserved.

The application of an external magnetic field H leads to canting of the magnetization vectors of the sublattices. Due to the s−f exchange coupling between electrons of the collectivized and localized subsystems, this cant induces a change in the spectral characteristics of the system. The form of these changes in the vicinity of the localized level is demonstrated in Fig. 5. The model parameters were chosen the same as in the previous calculation and the tem-
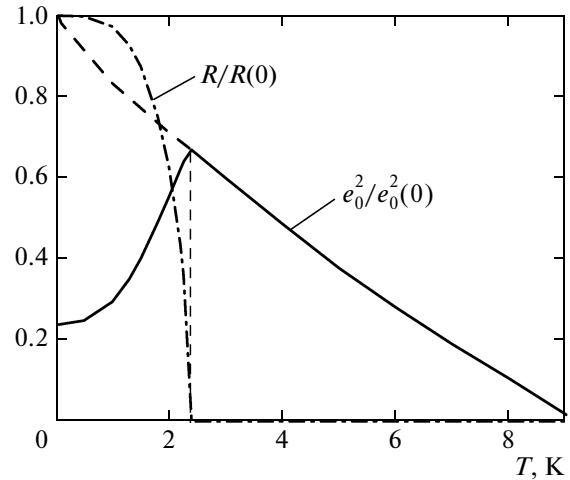

Fig. 3. Temperature dependences of relative renorm factor e_0^2 and relative sublattice magnetization for $|t_1| = 1$ eV.

perature was fixed at $T = 1$ K. The field of the spin-flip transition for the chosen parameters is $\mu_B H_c = 8.1 \times 10^{-3}$. Figure 5a shows the spectrum of quasiparticles calculated for $H/H_c = 0.214$. Comparison of this spectrum with the spectrum calculated for $H = 0$ (see Fig. 4a) shows that variation of the spectrum is observed in two cases. The first modification is of simple origin and associated with the removal of degeneracy in quantum number σ. The second feature is manifested as follows: for $\sigma = -1/2$, regions can be singled out on the first ($\lambda = 1$) and second ($\lambda = 2$) spectral branches, which come closer upon an increase in the magnetic field, while for $\sigma = +1/2$, analogous convergence is observed for the second ($\lambda = 2$) and third ($\lambda = 3$) branches. With a further increase in the magnetic field, this convergence of spectral regions is enhanced (Fig. 5b). For $H = H_c$ (Fig. 5c), the first and second spectral branched for $\sigma = -1/2$, as well as the second and third branches for $\sigma = +1/2$, come in contact. As a result, we obtain a spectral structure corresponding to the ferromagnetic phase for which the splitting in the projection of spin moment σ is induced by the effective field. Note that this is observed for the same value of the magnetic field for which the antiferromagnetism vector turns zero.

Analysis of the dispersion curves in Figs. 4 and 5 shows that a distinguishing feature of the Fermi quasiparticle spectrum with a canted AFM phase as compared to the HF spectrum in the para- and ferromagnetic phases is the presence of a narrow split band $E_{2k\sigma}$ with a structure quite sensitive to slight variations in temperature and magnetic field. The scale of the split band width, as well as the scales of fields and temperatures considerably affecting this band, is determined by exchange and s−f exchange integrals as well as the value of magnetization R. In the case when the chemical potential lies in the narrow band, the low-temper-
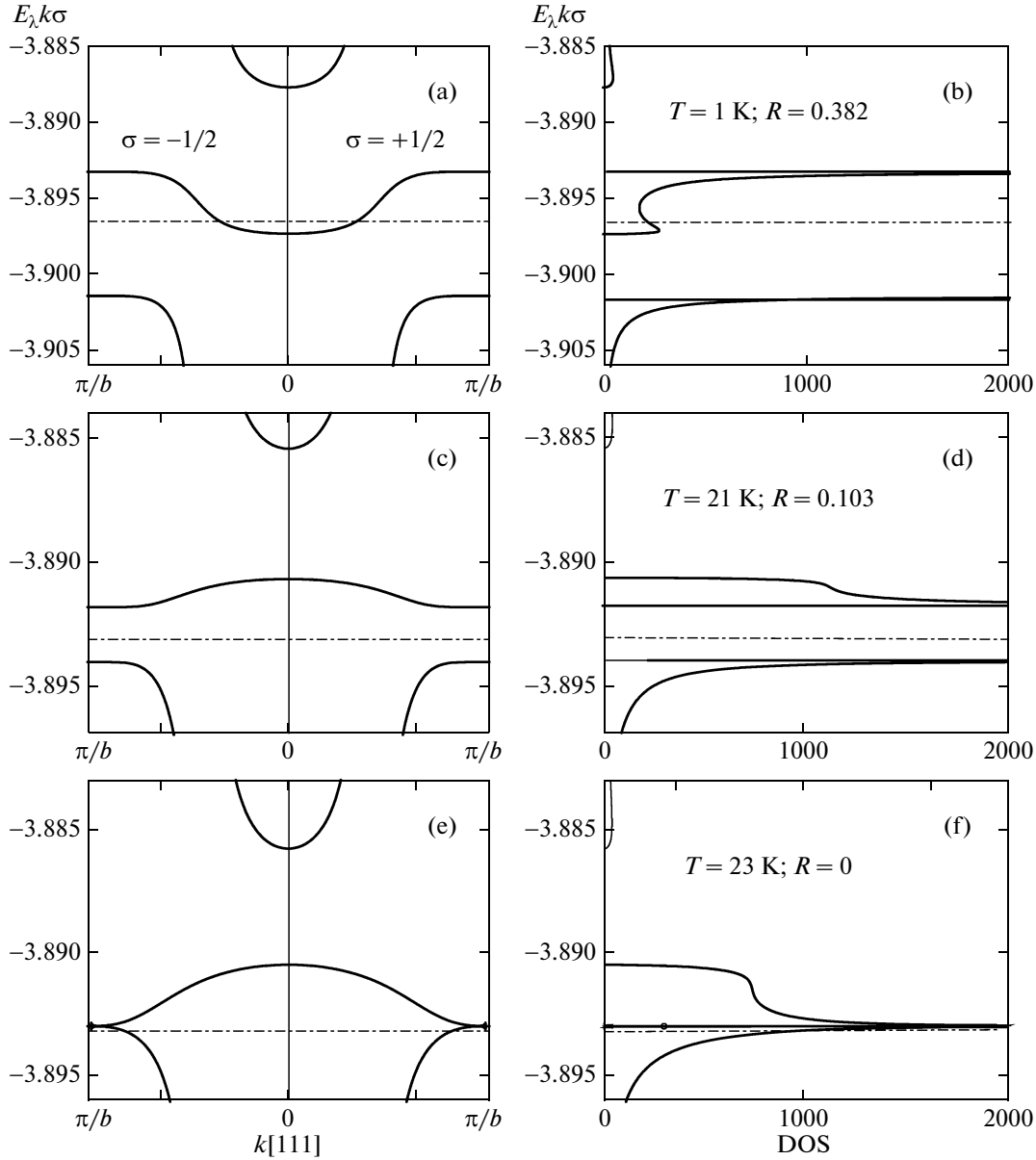
Fig. 4. Temperature evolution of (a, c, e) the Fermi spectrum and (b, d, f) density of electron states in the EPAM for the AFM phase in the vicinity of the localized level. The dot-and-dash line denotes the chemical potential. The Néel temperature is $T_N \approx 23$ K.

ature thermodynamics of the system is determined to a considerable extent by spectrum $E_{2k\sigma}$.

The results for the collinear and canted AFM phases were obtained from numerical solution of two ($\sigma = \pm 1/2$) fourth-order dispersion equations (25) describing the Fermi excitation spectrum $E_{\lambda k\sigma}$ for an arbitrary relation between parameters. In the case important for practical application in which the characteristic energy of splitting is much smaller that the width of the bare conduction band ($\overline{H}_\Lambda \ll W$), the expressions for the spectrum of heavy fermions described by branches $E_{2k\sigma}$ can be obtained in analytic

form. Indeed, if $\overline{H}_\Lambda \ll W$, we can state that $\xi^\pm_{k\sigma} = \pm|\Gamma_k|$ to a high degree of accuracy. In this case, to find the elementary excitation spectrum in the vicinity of the localized energy level $\zeta = E_0 + \lambda$, we can set $(\omega - \xi^\pm_{k\sigma}) \approx (\zeta \mp |\Gamma_k|)$ in dispersion equation (25). In this case, dispersion equation (25) assumes the form of a quadratic equation, and its two solutions

$$\Omega^\pm_{k\sigma} = \zeta(1 - \gamma_k) \pm \eta_{k\sigma},$$

$$\gamma_k = |\tilde{V}_k|^2/(\Gamma_k^2 - \zeta^2),$$

$$\eta_{k\sigma} = \{(\gamma_k\Gamma_k)^2 + \gamma_k(\Delta_\perp h_\perp - 2\sigma h_\parallel \Gamma_k$$
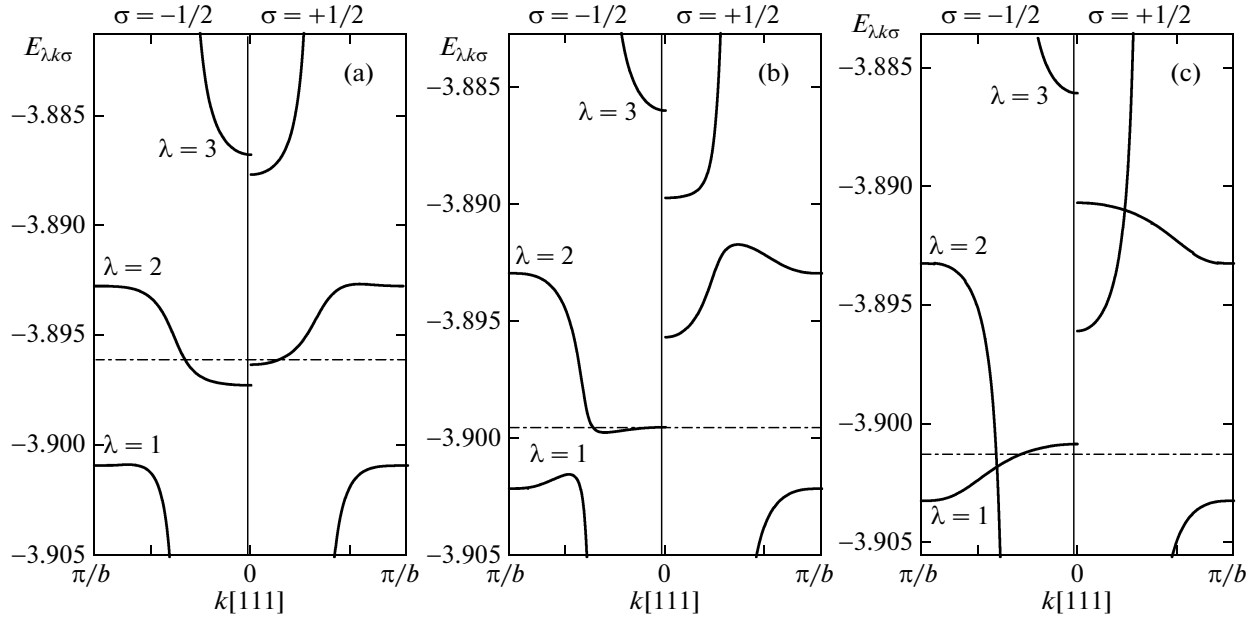
(37)

Fig. 5. Quasiparticle spectrum of an HF antiferromagnet in the canted phase in the vicinity of the localized level for various values of magnetic field: (a) $H/H_c = 0.214$, $R = 0.379$; (b) $H/H_c = 0.821$, $R = 0.391$; (c) $H/H_c = 1$, $R = 0.393$. The dot-and-dash line shows the position of the chemical potential.

$$- h_{\parallel}(J_0 R_{\parallel} - 2\mu_B H)/2) + \overline{H}_{\Lambda}^2/4 \}^{1/2},$$

describe the dispersion of Fermi excitations in this energy range. The solid (dashed) curves on the right-hand side of Fig. 6 describe the behavior of the energy spectrum defined by solutions $\Omega_{k,+1/2}^{-}$ ($\Omega_{k,+1/2}^{+}$). The model parameters were chosen the same as in calculation of the curves in Figs. 4 and 5. In this case, field $H = 0$ and temperature $T = 1$ K. The dotted curve on the left-hand side of Fig. 6 shows the branches of the $E_{\lambda k, -1/2}$ spectrum calculated from dispersion equation (25). In the collinear AFM phase, the spectrum is degenerate in quantum number σ: $E_{\lambda k, -1/2} = E_{\lambda k, +1/2}$. Consequently, if our approximation is justified, the dispersion curves on the left and right sides of Fig. 6 must coincide. It can be seen from comparison of the curves that the behavior of the energy spectrum in the vicinity of the localized level, which is described by analytic expressions (37), is practically indistinguishable from the spectrum determined from the exact solution to the dispersion equation. A discrepancy appears only in the energy range beyond the neighborhood of ζ and is not seen in the given figure.

Note that the mean dispersion curve on the right-hand side of Fig. 6, which is represented by a solid curve that transforms into a dotted curve, is associated with the discontinuous type of solutions (37) at point $k = k_c$ at which γ_k reverses its sign. In the region $k < k_c$, branch $\Omega_{k,\sigma}^{+}$ corresponds to the $E_{3k\sigma}$ branch, while for $k > k_c$, it corresponds to the branch with $\lambda = 2$. Branch

$\Omega_{k,\sigma}^{-}$ for $k < k_c$ corresponds to the $E_{2k\sigma}$ branch, while in the range of large values of quasi-momentum, it corresponds to the $E_{1k\sigma}$ branch. On account of such behavior, we can write the analytic expression for the spectrum of the split HF band in the form

$$E_{2k\sigma} = \zeta(1 - \gamma_k) - \text{sgn}(\gamma_k)\eta_{k\sigma}. \qquad (38)$$

It should be emphasized that this expression holds in the entire range of magnetic fields in which the canted phase of AFM intermetallide is formed. All dispersion
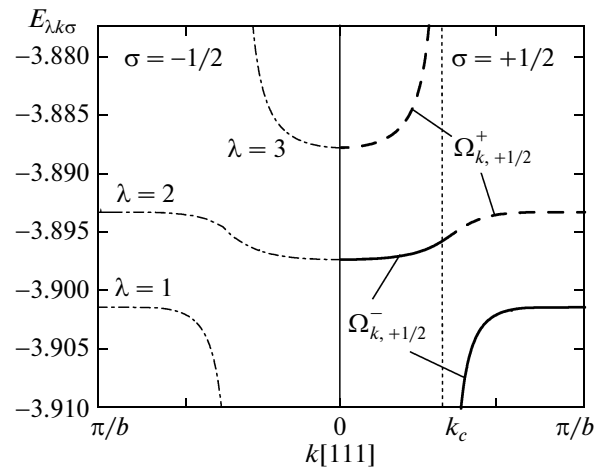

Fig. 6. Quasiparticle spectrum of an HF antiferromagnet in the collinear AFM phase in the vicinity of the localized level, calculated from fourth-degree dispersion equation (25) (for $\sigma = -1/2$) and by formula (37) (for $\sigma = +1/2$).
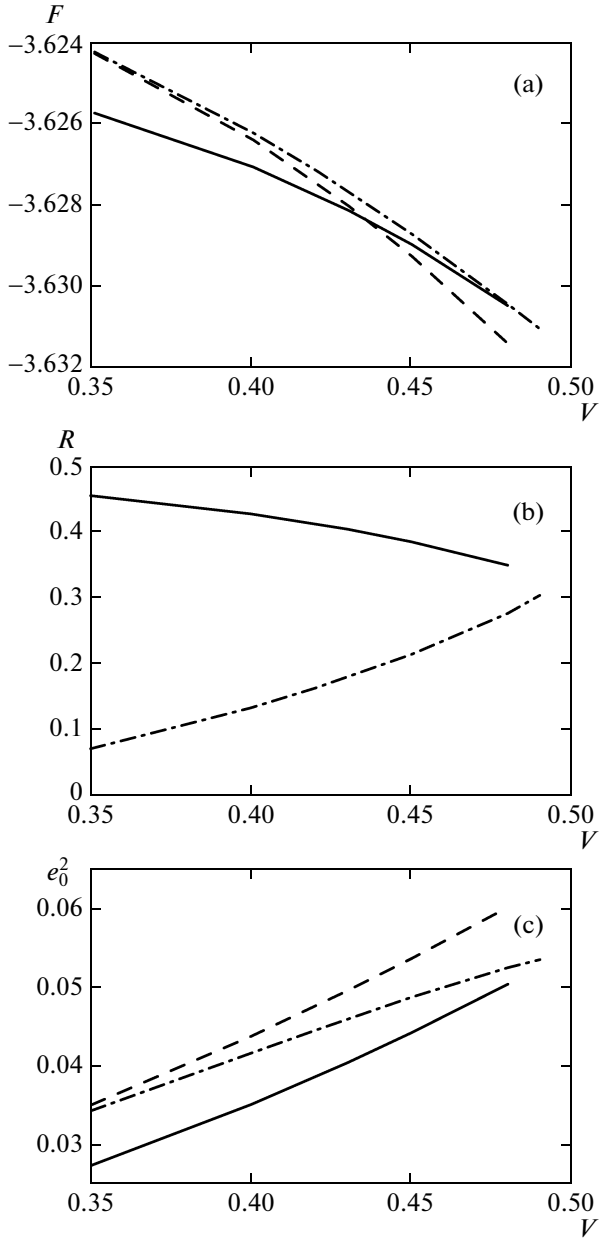
Fig. 7. (a) Free energy of the paramagnetic (dashed curve) and two AFM (solid and dot-and-dash curve) solutions; (b) behavior of the order parameters for two AFM phases; (c) renorm parameter e_0^2.

curves with $\lambda = 2$ shown in Figs. 4 and 5 are successfully described by analytic expression (38).

In particular cases of the AFM, ferromagnetic (FM), and paramagnetic phases (PM), Eq. (38) gives

$$E_{2k\sigma}^{\text{AFM}} = \zeta(1 - \gamma_k) - \text{sgn}(\gamma_k)$$

$$\times \left\{ (\gamma_k \Gamma_k)^2 + \gamma_k \Delta_\perp h_\perp + h_\perp^2/4 \right\}^{1/2},$$

$$E_{2k\sigma}^{\text{FM}} = \zeta(1 - \gamma_k) - \text{sgn}(\gamma_k) \left\{ (\gamma_k \Gamma_k - \sigma h_\parallel)^2 \quad (39) \right.$$

$$\left. - \frac{h_\parallel \gamma_k}{2}(J_0 R_\parallel - 2\mu_B H) \right\}^{1/2}, \quad H \geq H_c,$$

$$E_{2k\sigma}^{PM} = \zeta + \frac{|\tilde{V}_k|^2}{\Gamma_k + \zeta}.$$

Formula (38) makes it possible to also derive an expression for effective mass m^* of heavy quasiparticles in the canted AFM phase. Expanding relation (38) in the vicinity of small k, we obtain

$$\frac{m^*}{m_0} = \frac{\Gamma_0^2 - \zeta^2}{|\Gamma_0|\gamma_0}$$

$$\times \left\{ 2|\zeta| - \left[\Delta_\perp h_\perp - h_\parallel(J_0 R_\parallel - 2\mu_B H)/2 \right. \right. \quad (40)$$

$$\left. \left. + (\Gamma_0^2 + \zeta^2)\left(\gamma_0 + \sigma\frac{h_\parallel}{|\Gamma_0|}\right) \right]/\eta_{0\sigma} \right\}^{-1},$$

where m_0 is the effective mass of bare collectivized electrons in the vicinity of the bottom of the band. For dispersion relation (36), mass m_0 can be determined from the expression $\hbar^2/2m_0 b^2 = |t_1|$. In the paramagnetic phase, we obtain the following simple relation for the effective mass of heavy quasiparticles:

$$\frac{m_{\text{PM}}}{m_0} = -\frac{(|\Gamma_0| + |\zeta|)^2}{|V|^2(1 - n_f)}. \quad (41)$$

The negativeness of the mass is responsible for the hole nature of heavy quasiparticles in the paraphase.

6. THERMODYNAMIC PROPERTIES OF HF INTERMETALLIDES IN THE CANTED AFM PHASE

Numerical analysis of self-consistent equations shows that for a given set of model parameters and external conditions, several stable phases can form. The choice of the stable state from metastable states is dictated by the lowest value of free energy. Taking into account relations (7) and (22), we can write the following expression for free energy:

$$F(T, V, N)$$

$$= -T\sum_{\lambda = 1}^{4}\sum_{k\sigma}\ln\left(1 + \exp\left\{-\frac{E_{\lambda k\sigma} + \mu}{T}\right\}\right) + C + \mu N. \quad (42)$$

Calculations show that the intensity of hybridization processes affects the result of competition between the AFM and PM phases. The change of the type of state upon an increase in the hybridization parameter is illustrated in Fig. 7. Calculations were performed for the following parameters: $E_0 = -2$, $K_0 = 0.02$, $J_0 = 0.5$, $n = 2.8$, $T = 1$ K, and $H = 0$. Figure 7 shows that for a hybridization parameter smaller than $V_c \approx 0.43$, the

AFM phase with the strongest magnetization is stable. However, for $V > V_c$, the stable phase corresponds to the paramagnetic solution with $R = 0$, while solutions of the AFM type become metastable. Such a variation of the stable phase of the system upon an increase in the hybridization parameter is a particular case of the first-order transition in the interaction parameter. For zero temperature, this would correspond to a quantum phase transition. Knowing the variation in the structure of the GS of the system upon an increase in V, we can describe the evolution of the band structure upon an increase in the intensity of hybridization processes. For small values of V, the Fermi excitation spectrum in the vicinity of the localized level has the form typical of AFM ordering in the system (see Fig. 4a). With an increasing hybridization parameter, the narrow band shrinks and the hybridization gaps become wider. For $V = V_c$, when the type of the ground state changes from AFM to paramagnetic, the elementary excitation spectrum acquires the form shown in Fig. 4e. It should be emphasized that the energy spectrum corresponding to states with heavy fermions is considerably modified in this case due to evolution of the long-range AFM order due to a change in the hybridization parameter. Rearrangement of magnetic ordering in the localized subsystem induces a variation in the spectral properties of Fermi quasiparticles. In this case, hybridization plays the role of a parameter controlling magnetization of the sublattices.

This scenario of jumpwise variation in the GS structure of the localized subsystem upon an increase in the hybridization parameter is not unique. Choosing other values of the model parameters, we can create conditions in which the AFM state remains a stable phase down to very small values of sublattice magnetization. This means that a transition from magnetically ordered to the paramagnetic state may occur via a second-order transition or via a first-order phase transition close to the second-order transition. This type of evolution of the parameters of the stable phase is illustrated in Fig. 8. In this case, calculations were performed with different values of the bare energy of the localized level and electron concentration ($E_0 = -4$ and $n = 2.2$). The remaining model parameters were chosen the same as in calculations of the curves in Fig. 7. It can be seen that for all values of V, the solution describing the long-range magnetic order corresponds to a lower energy than that for the paramagnetic state. However, the value of magnetic moment R decreases from $R = 0.45$ (for $V = 0.1$) to $R = 0.06$ (for $V = 0.7$). It should be noted in this connection that it is precisely such small values of the sublattice magnetization that are observed in experiments with many HF antiferromagnets.

Our analysis of the Fermi excitation spectrum in the AFM phase corresponds to the electron concentration for which chemical potential μ is within the narrow split-off band. The conditions for the existence of the AFM solutions are observed precisely in this
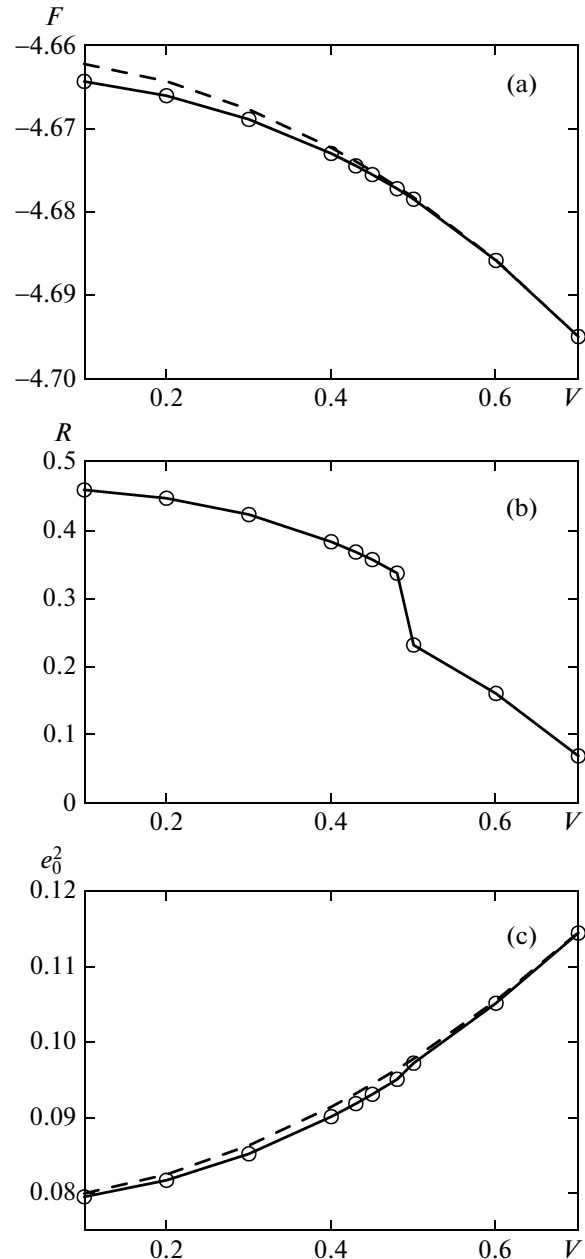

Fig. 8. Dependences of (a) free energy F, (b) AFM order parameter R, and (c) renorm parameter on hybridization V for the paramagnetic solution (dashed curve) and the AFM solution (solid curve).

case. Upon an increase in electron concentration n, localized states become depleted and lattice magnetization R decreases. The changes in the spectral structure and in the density of states emerging in this case in the vicinity of the localized level are demonstrated in Fig. 9. The model parameters used in calculating these curves were as follows: $E_0 = -4$, $V = 0.7$, $K_0 = 0.02$, and $J_0 = 0.5$. The temperature was chosen at 1 K, and the magnetic field was zero. For $n = 2.4$ (Figs. 9a and 9b), the chemical potential is approximately at the
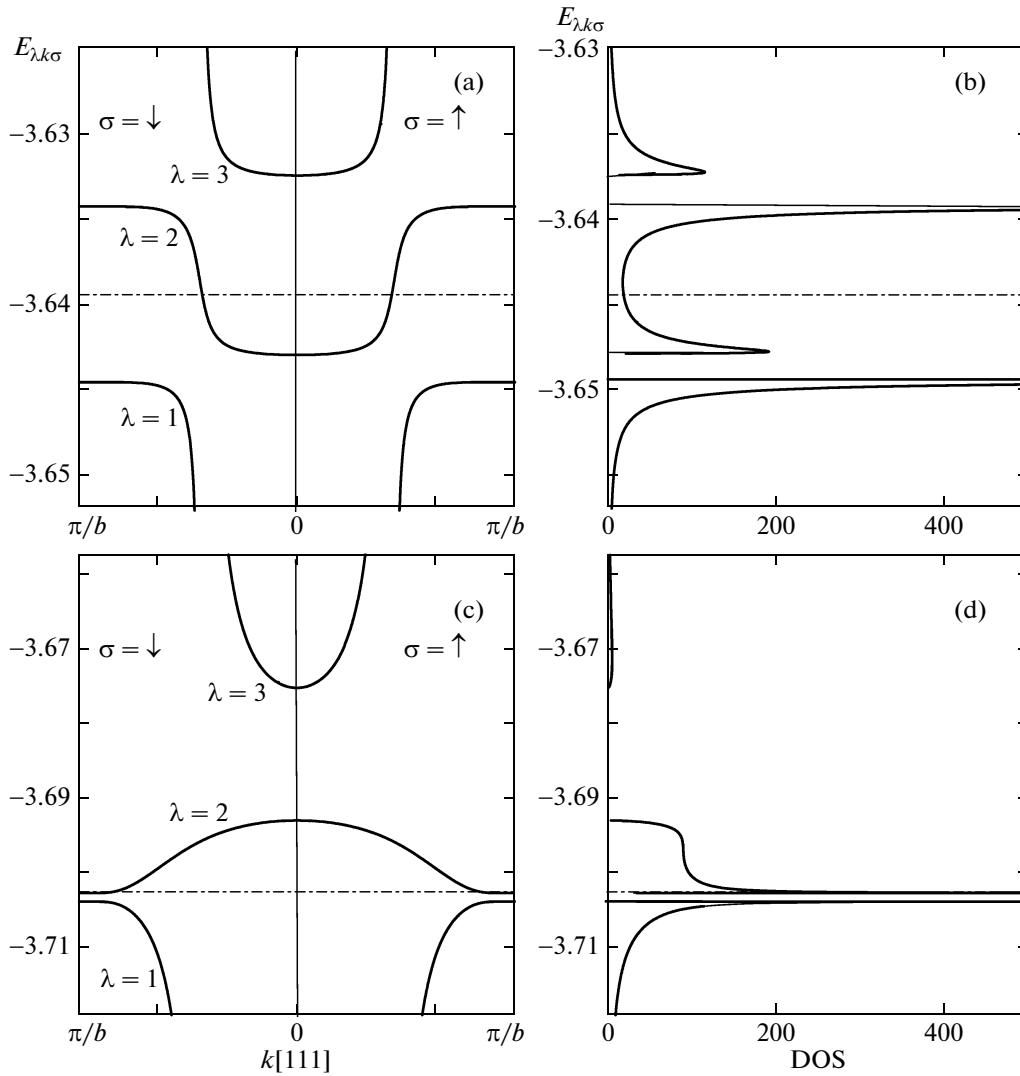
Fig. 9. Quasiparticle spectrum and density of states in the vicinity of the localized level for $n = 2.4$; $R = 0.460$ (a, b); $n = 2.2$, $R = 0.061$ (c, d).

middle of the narrow band between the peaks of the density of states (dot-and-dash curve). The system exhibits a long-range AFM order with a large magnetic moment of the rare-earth ion ($R = 0.460$). A decrease in the concentration to $n = 2.2$ (Figs. 9c and 9d) leads not only to a decrease in chemical potential μ, but also to a considerable rearrangement of the dispersion curve for the narrow band, which is manifested as a change in its curvature (inversion of the narrow band). As well, the upper gap increases, while the lower gap decreases but remains finite. From the point of view of physics, the observed inversion of the narrow band indicates the sign reversal of the effective mass.

The results of the above calculations show that a decrease in concentration n leads to substantial suppression of the magnetic moment down to $R = 0.061$, which, as noted above, correlates with the values of magnetization in many HF antiferromagnets. Another

important aspect is the displacement of the chemical potential so that it falls to the peak of the density of states (see Fig. 9d). This facilitates the formation of states with heavy fermions and strongly affects the thermodynamic properties of the system (in particular, the electron heat capacity of HF antiferromagnets).

Figure 10 shows the results of solving the system of self-consistent equations for various temperature values. The temperature dependences of sublattice magnetization R, heat capacity C of the system, and Sommerfeld constant $\gamma = C/T$ in zero magnetic field presented in the figure were obtained for two values of electron concentration ($n = 2.4$ and 2.2). The remaining model parameters were the same as for the curves plotted in Fig. 9. Comparison of Figs. 10a and 10d shows that upon a decrease in the concentration accompanied by a displacement of the chemical potential towards the peak of the density of states (see
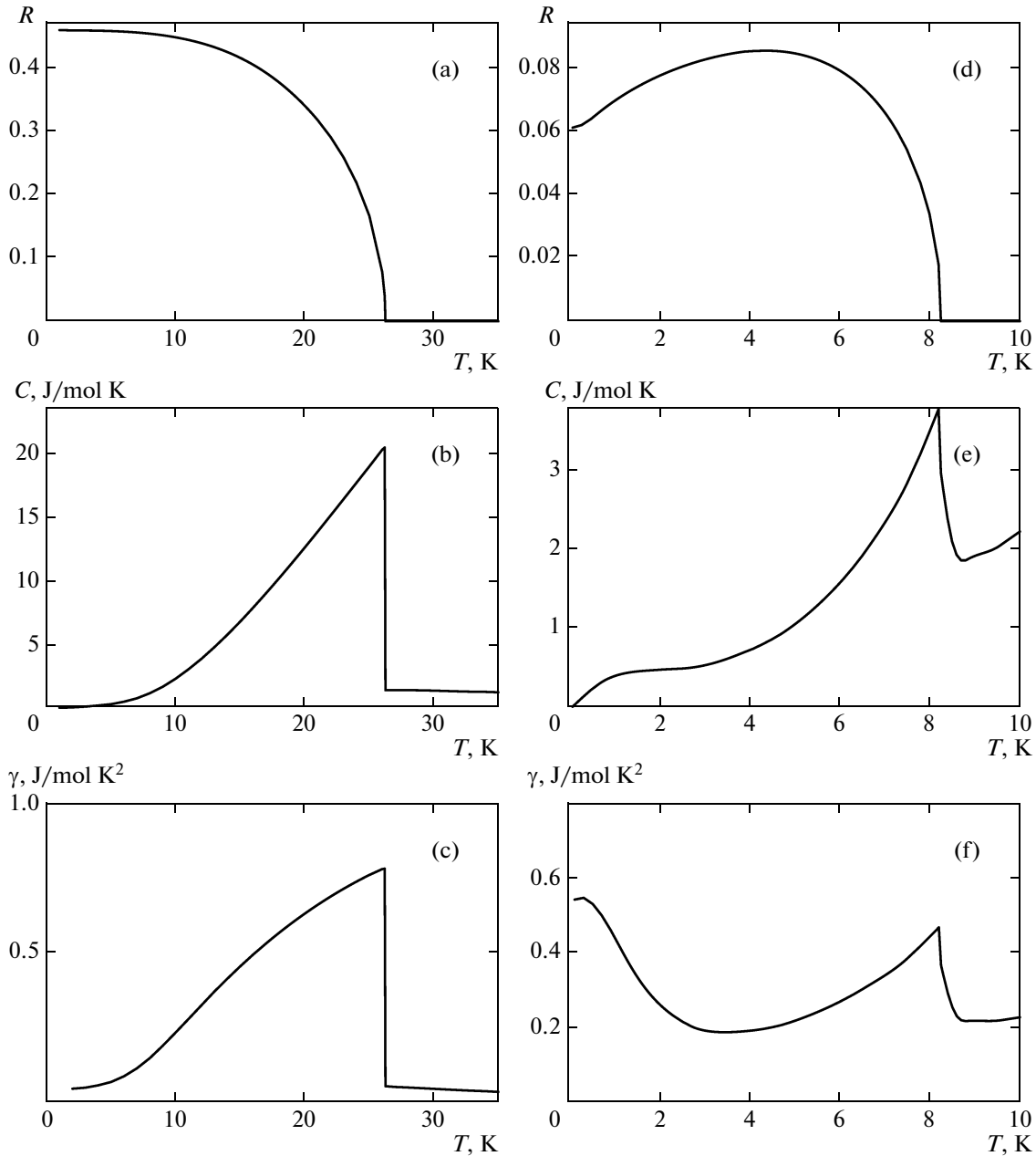
Fig. 10. Temperature dependence of magnetic moment R, heat capacity C, and Sommerfeld constant γ for two values of electron concentration: $n = 2.4$ (a, b, c) and 2.2 (d, e, f).

Fig. 9 and the notes to it), not only magnetic moment R decreases, but also the values of critical temperature: $T_N = 26.2$ K for $n = 2.4$ (see Fig. 10a) and $T_N = 8.2$ K for $n = 2.2$ (see Fig. 10d). It should be noted for comparison that the characteristic Néel temperature of classical HF antiferromagnets is approximately 10 K.

Figures 10b and 10e demonstrate a sharp change in the heat capacity of the system in the vicinity of the temperature of transition from the AFM to the paramagnetic phase. The strong increase in the value of C observed when T_N is approached from the left is due to the contribution of the magnetic degrees of freedom.

The existence of strong electron correlations in the system hampers the separation of the electronic and magnetic contributions to the thermodynamic parameters of HF antiferromagnets. However, at very low temperatures $T \ll T_N$, the electron heat capacity considerably exceeds the magnetic heat capacity. For this reason, ratio C/T makes it possible to estimate the effective mass of electrons and their density of states. This information can be obtained from Figs. 10c and 10f. For $n = 2.4$, at which the chemical potential is at the middle of the narrow band between the peaks of the density of states (see Fig. 9b), the heat capacity of
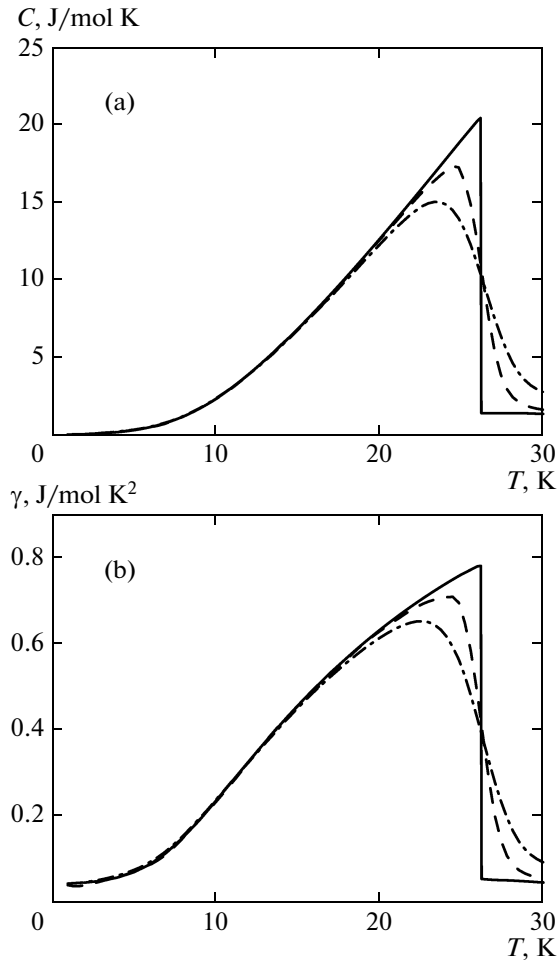
C, J/mol K

γ, J/mol K^2

Fig. 11. Temperature dependences of (a) heat capacity and (b) Sommerfeld constant for concentration $n = 2.4$ and for three values of magnetic field: $H = 0$ (solid curve), $\mu_B H = 5.79 \times 10^{-4}$ (dashed curve), and $\mu_B H = 1.16 \times 10^{-3}$ (dot-and-dash curve).

the system is approximately 50 times higher than the heat capacity of a gas of free electrons (see Fig. 10c). Such quasiparticles are treated as heavy, and the order of magnitude of their effective mass corresponds, for example, to the mass of charge carriers in HF skutterudite $LaFe_4P_{12}$ [13].

As the concentration decreases to $n = 2.2$, the chemical potential is shifted to the peak of the density of states (see Fig. 9d), and the electron heat capacity of the system increases by an order of magnitude (see Fig. 10f). This means that the effective mass of heavy quasiparticles in this regime attains a value of approximately 500 masses of a free electron. Such values of the quasiparticle mass are typical of classical HF systems.

Finally, we note that the temperature variations in constant γ for $n = 2.4$ and 2.2 are different. In the former case, the Sommerfeld constant increases monotonically up to T_N (see Fig. 10c), while in the lat-

ter case, it first decreases and then increases (see Fig. 10f).

It was noted above that the application of a magnetic field cants the magnetizations of the sublattices. This induces a modification of the spectral curves and a change in the density of states. The rearrangement of the GS must obviously affect the thermodynamic properties of the system. Figure 11 shows the calculated temperature dependences of the heat capacity and parameter γ for $n = 2.4$ for three values of the magnetic field below the spin-flip transition point. The model parameters were chosen the same as those used for calculating the curves in Fig. 10. It can be seen from Fig. 11 that the application of the magnetic field not only blurs the phase-transition region, but also reduces the value of temperature T_{max} corresponding to the heat capacity peak on the $C(T)$ curve. This points to a decrease in the Néel temperature since it is precisely T_{max} that is interpreted in experiment as the AFM transition temperature. Such a behavior of the $C(T)$ and $\gamma(T)$ dependences was observed in experiments with $PuGa_3$ [24], Ce_2Au_2Cd [25], $YbNiSi_3$ [26], and $PuPd_5Al_2$ systems [25].

7. CONCLUSIONS

The main results of this study can be summarized as follows.

1. The slave-boson representation has been used for the first time to consider the spectral and thermodynamic properties of AFM intermetallides with heavy fermions, in which a magnetic field cants magnetic sublattices. To derive the dispersion equation describing the branch of the Fermi-type elementary excitation spectrum in the canted AFM phase, a sequence of unitary transformation was employed. Such an approach was employed to represent the eighth-order determinant in an explicit block-diagonal form in terms of two fourth-order determinants. The application of this program radically simplified not only the analytic part of the problem, but also the numerical calculations involving the solution of a large number of transcendental self-consistent equations.

2. The calculations revealed the features of formation of the heavy-fermion spectrum in rare-earth intermetallides with AFM ordering of spin moments of the localized subsystem. In particular, it was shown that the state of heavy fermions in such systems corresponds to a narrow band separated by energy gaps from above and below. The magnetic field inducing the canting of the magnetic sublattices considerably modifies the dispersion relation for this band and leads to a change in the effective mass not only in magnitude, but also in sign.

3. For the first time, an analytic expression describing the HF spectrum in wide ranges of magnetic fields and temperatures were obtained for the noncollinear phase with a nonzero antiferromagnetism vector. This enabled us to establish explicit relations between the

effective masses for the paramagnetic phase and collinear AFM phase, as well as the ferromagnetic phase formed in the range of strong magnetic fields after the spin-flop transition.

4. The effect of magnetic degrees of freedom of collectivized electrons on canting of sublattice magnetizations in a magnetic field was taken into account. This circumstance is especially important for HF compounds with the metal-type ground state, in which the charge carrier concentration is high. It is found, in particular, that the thermodynamic principles can be observed in the low-temperature range only in the framework of such a description.

5. The expressions obtained for the spectrum of heavy fermions in various phases were used for analyzing the thermodynamic behavior of the system. The dependences of the sublattice magnetization and free energy on the controlling parameters and temperature were calculated. It was noted for the first time that the existence of magnetic ordering leads to a qualitative change in the temperature dependence of the renorm factor e_0^2 in the slave-boson representation. In the AFM phase, the value of e_0^2 increases monotonically with temperature. The ranges of parameters in which the magnetization of the sublattice assumes small values corresponding to experimental data on AFM HF intermetallides have been determined.

6. For the first time, canting of magnetic sublattices was taken into account in analyzing the behavior of heat capacity in the noncollinear AFM phase. It was shown that the changes in the electron heat capacity induced by the magnetic field correlate with the available experimental data on AFM intermetallides.

ACKNOWLEDGMENTS

REFERENCES

1. A. Amato, Rev. Mod. Phys. **69**, 1119 (1997).

2. T. Takabatake, F. Teshima, H. Fujii, S. Nishigori, T. Suzuki, T. Fujita, Y. Yamaguchi, J. Sakurai, and D. Jaccard, Phys. Rev. B: Condens. Matter **41**, 9607 (1990).

3. K. A. Kikoin, M. N. Kiselev, A. S. Mishchenko, and A. de Visser, Phys. Rev. B: Condens. Matter **59**, 15070 (1999).

4. L. Degiorgi, Rev. Mod. Phys. **71**, 687 (1999).

5. H. Sugawara, S. Osaki, M. Kobayashi, T. Namiki, S. R. Saha, Y. Aoki, and H. Sato, Phys. Rev. B: Condens. Matter **71**, 125 127 (2005).

6. Yu. Kagan, K. A. Kikoin, and N. V. Prokof'ev, Physica B (Amsterdam) **182**, 201 (1992).

7. Yu. Kagan, K. A. Kikoin, and N. V. Prokof'ev, Pis'ma Zh. Éksp. Teor. Fiz. **56** (4), 221 (1992) [JETP Lett. **56** (4), 219 (1992)].

8. F. Steglich, J. Aarts, C. D. Bredl, W. Lieke, D. Meschede, W. Franz, and H. Schafer, Phys. Rev. Lett. **43**, 1892 (1979).

9. H. R. Ott, H. Rudigier, Z. Fisk, and J. L. Smith, Phys. Rev. Lett. **50**, 1595 (1983).

10. G. R. Stewart, Z. Fisk, J. O. Willis, and J. L. Smith, Phys. Rev. Lett. **52**, 679 (1984).

11. C. Petrovic, R. Movshovich, M. Jaime, P. G. Pagliuso, M. F. Hundley, J. L. Sarrao, Z. Fisk, and J. D. Thompson, Europhys. Lett. **53**, 354 (2001).

12. H. Hegger, C. Petrovic, E. G. Moshopoulou, M. F. Hundley, J. L. Sarrao, Z. Fisk, and J. D. Thompson, Phys. Rev. Lett. **84**, 4986 (2000).

13. Y. Nakai, K. Ishida, D. Kikuchi, H. Sugawara, and H. Sato, J. Phys. Soc. Jpn. **74**, 3370 (2005).

14. T. Namiki, Y. Aoki, H. Sato, C. Sekine, I. Shirotani, T. Matsuda, Y. Haga, and T. Yagi, J. Phys. Soc. Jpn. **76**, 093 704 (2007).

15. E. Vergoz and D. Jaccard, J. Magn. Magn. Mater. **177–181**, 294 (1998).

16. S. S. Saxena, P. Agarwal, K. Ahilan, F. M. Grosche, R. K. W. Haselwimmer, M. J. Steiner, E. Pugh, I. R. Walker, S. R. Julian, P. Monthoux, G. G. Lonzarich, A. Huxley, I. Sheikin, D. Braithwaite, and J. Flouquet, Nature (London) **406**, 587 (2000).

17. T. Akazawa, H. Hidaka, H. Kotegawa, T. C. Kobayashi, T. Fujiwara, E. Yamamoto, Y. Haga, R. Settai, and Y. Onuki, J. Phys.: Condens. Matter **16**, L29 (2004).

18. C. Pfleiderer, M. Uhlarz, S. M. Hayden, R. Vollmer, H. V. Lohneysen, N. R. Bernhoeft, and G. G. Lonzarich, Nature (London) **412**, 58 (2001).

19. T. Park, F. Ronning, H. Q. Yuan, M. B. Salamon, R. Movshovich, J. L. Sarrao, and J. D. Thompson, Nature (London) **440**, 65 (2006).

20. P. A. Alekseev, J.-M. Mignot, K. S. Nemkovskiĭ, V. N. Lazukov, E. V. Nefedova, A. P. Menushenkov, A. V. Kuznetsov, R. I. Bewley, and A. V. Gribanov, Zh. Éksp. Teor. Fiz. **132** (1), 22 (2007) [JETP **105** (1), 14 (2007)].

21. A. V. Bogach, G. S. Burkhanov, V. V. Glushkov, S. V. Demishev, O. D. Chistyakov, and N. E. Sluchanko, Zh. Éksp. Teor. Fiz. **132** (1), 125 (2007) [JETP **105** (1), 108 (2007)].

22. N. E. Sluchanko, A. V. Bogach, V. V. Glushkov, S. V. Demishev, N. A. Samarin, G. S. Burkhanov, and O. D. Chistyakov, Pis'ma Zh. Éksp. Teor. Fiz. **76** (1), 31 (2002) [JETP Lett. **76** (1), 26 (2002)].

23. M. I. Ignatov, A. V. Bogach, G. S. Burkhanov, V. V. Glushkov, S. V. Demishev, A. V. Kuznetsov, O. D. Chistyakov, N. Yu. Shitsevalova, and N. E. Sluchanko, Zh. Éksp. Teor. Fiz. **132** (1), 69 (2007) [JETP **105** (1), 58 (2007)].

24. P. Boulet, E. Colineau, F. Wastin, P. Javorsky, J. C. Griveau, J. Rebizant, G. R. Stewart, and E. D. Bauer, Phys. Rev. B: Condens. Matter **72**, 064438 (2005).

25. S. Rayaprol and R. Pottgen, Phys. Rev. B: Condens. Matter **72**, 214 435 (2005).

26. S. L. Bud'ko, P. C. Canfield, M. A. Avila, and T. Takabatake, Phys. Rev. B: Condens. Matter **75**, 094 433 (2007).

27. K. Gofryk, J.-C. Griveau, E. Colineau, and J. Rebizant, Phys. Rev. B: Condens. Matter **77**, 092 405 (2008).

28. P. Misra, *Heavy Fermion Systems* (Elsevier, Oxford, 2008).

29. V. Dorin and P. Schlottmann, Phys. Rev. B: Condens. Matter **46**, 10 800 (1992).

30. B. Moller and P. Wolfle, Phys. Rev. B: Condens. Matter **48**, 10 320 (1993).

31. E. Halvorsen and G. Czycholl, J. Phys.: Condens. Matter **8**, 1775 (1996).

32. S.-J. Sun, M.-F. Yang, and T.-M. Hong, Phys. Rev. B: Condens. Matter **48**, 16 127 (1993).

33. J. R. Schrieffer and P. A. Wolff, Phys. Rev. **149**, 491 (1966).

34. C. Lacroix and M. Cyrot, Phys. Rev. B: Condens. Matter **20**, 1969 (1979).

35. V. A. Moskalenko and N. B. Perkins, Teor. Mat. Fiz. **121** (3), 464 (1999) [Theor. Math. Phys. **121** (3), 1654 (1999)].

36. D. F. Digor, P. Entel, M. Marinaro, V. A. Moskalenko, and N. B. Perkins, Teor. Mat. Fiz. **127** (2), 304 (2001) [Theor. Math. Phys. **127** (2), 664 (2001)].

37. Z. Liang-Jian and Z. Qing-Qi, J. Magn. Magn. Mater. **109**, 237 (1992).

38. V. V. Val'kov and D. M. Dzebisashvili, Teor. Mat. Fiz. **157** (2), 235 (2008) [Theor. Math. Phys. **157** (2), 1565 (2008)].

39. P. Coleman, Phys. Rev. B: Condens. Matter **29**, 3035 (1984).

40. A. Grauel, A. Böhm, H. Fischer, C. Geibel, R. Köhler, R. Modler, C. Schank, F. Steglich, G. Weber, T. Komatsubara, and N. Sato, Phys. Rev. B: Condens. Matter **46**, 5818 (1992).

41. R. Movshovich, T. Graf, D. Mandrus, J. D. Thompson, J. L. Smith, and Z. Fisk, Phys. Rev. B: Condens. Matter **53**, 8241 (1996).

Translated by N. Wadhwa